Available online at www.sciencedirect.com
SCIENCE DIRECT
Acta Materialia 54 (2006) 1165–1173
Acta MATERIALIA
www.actamat-journals.com

# Micrograph evidence of meniscus solidification and sub-surface microstructure evolution in continuous-cast ultralow-carbon steels

J. Sengupta [a], H.-J. Shin [b], B.G. Thomas [a,*], S.-H. Kim [b]

[a] *Department of Mechanical and Industrial Engineering, University of Illinois at Urbana-Champaign, 1206 West Green Street, Urbana, IL 61801, USA*
[b] *Department of Materials Science and Engineering, Pohang University of Science and Technology (POSTECH), Pohang, Kyungbuk 790-784, Republic of Korea*

Received 10 August 2005; received in revised form 15 October 2005; accepted 17 October 2005
Available online 3 January 2006

**Abstract**

Hooks and other sub-surface features in continuous-cast ultralow-carbon steel samples were examined using optical microscopy, electron backscattering diffraction, energy dispersive X-ray spectroscopy, and electron probe microanalysis techniques. Special etching reagents revealed dendrites growing from both sides of the line of hook origin. This line was found to represent the frozen meniscus and persisted into the final microstructure, as revealed by grain orientation measurements. A broken hook tip was observed in one micrograph, which explains the characteristic truncated shape of most hooks. Mold powder was found entrapped along the frozen meniscus. These results provide evidence of both solidification and subsequent overflow of the liquid steel meniscus. Thus, the instantaneous meniscus shape governs the shape and microstructure of the final hook, and the extent of the liquid steel overflow determines the shape of oscillation marks. This mechanism has important implications for the entrapment of inclusions and other surface defects.


*Keywords:* Casting; EBSD; SEM; Solidification microstructure; Ultralow-carbon steel

## 1. Introduction

Periodic transverse depressions called "oscillation marks" (OMs), shown in Fig. 1 (front view of a slab), are routinely observed on the surface of steel slabs manufactured by continuous casting processes [1–3]. Additionally, a distinctive sub-surface microstructural feature called a "hook" often accompanies deep OMs in steels with low (<0.1%) carbon contents [4,5]. This feature occurring within ~2–4 mm below the slab surface is difficult to distinguish using conventional etching methods.

Severe hook and OM formation degrades the slab surface quality owing to the entrapment of argon bubbles and alumina inclusions near the hooks [6,7], and the formation of transverse cracks near the roots of OMs [1,3,8]. Transverse cracks initiate due to the coarser grain structure and the presence of embrittling precipitates often found in this region [3,8]. In extreme cases, the entire slab surface must be ground or "scarfed" to remove completely these defects, resulting in loss of productivity [9].

The formation of hooks and OMs is associated with the vertical oscillation of the water-cooled copper mold, which significantly alters the local heat transfer, fluid flow, and initial solidification in the meniscus region. This oscillation is required to facilitate smooth withdrawal of the solidifying steel shell from the mold by preventing the shell from sticking to the mold wall. This is aided by a "negative strip time" period during the cycle, when the mold moves downward faster than the casting speed. Oscillation also pumps molten flux into the gap formed between the shell and mold faces, where it acts as a lubricant.

* Corresponding author. Tel.: +1 217 333 6919; fax: +1 217 244 6534.
*E-mail address:* bgthomas@uiuc.edu (B.G. Thomas).

1359-6454/$30.00 
doi:10.1016/j.actamat.2005.10.044

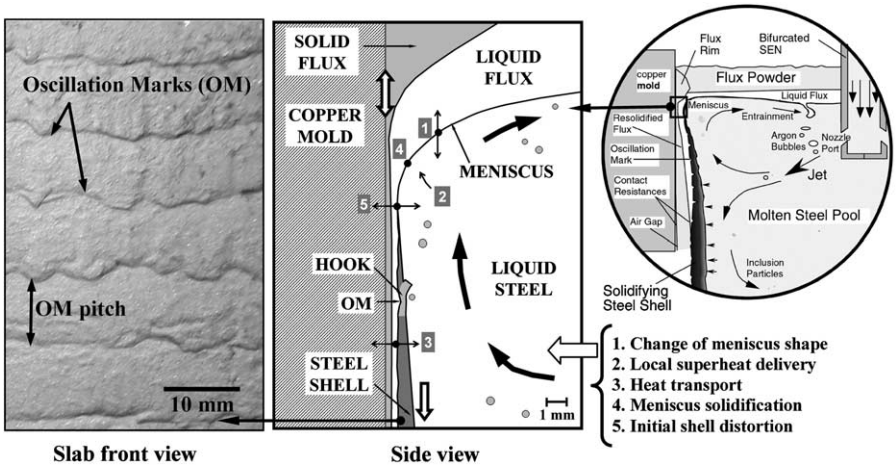


Fig. 1. Inside a continuous caster mold (right), a range of complex phenomena in the meniscus region (middle) creates periodic oscillation marks (left) on the slab surface.

The flux is added as a powder to the top free surface of the liquid steel pool. It melts to create a continuous liquid flux layer (see Fig. 1) that conforms to the steel surface contour and flow field, and provides thermal and chemical insulation to the liquid steel. In addition to the mold oscillation frequency and stroke, many different parameters affect OM formation, including the casting speed, superheat temperature difference, and liquid steel flow pattern in the mold.

Several studies focusing on low-, medium-, and high-carbon steels have been conducted in the past to explain hook and OM formation, which is crucial for optimizing casting conditions and improving the process. Most of the mechanisms proposed so far are based on transient events occurring near the meniscus, which involve a range of complex, inter-related phenomena illustrated in Fig. 1. Pressure fluctuations in the liquid flux channel dynamically alter the meniscus shape. The turbulent flow pattern in the mold cavity brings liquid to the meniscus region with varying amounts of superheat. Heat is conducted from the solidification front to the mold through the steel shell and the interfacial gap, which consists of liquid and re-solidified layers of mold flux. The meniscus region might solidify, depending on the local superheat of the liquid, the availability of nucleation sites, the ease of nucleation and growth, and alloy properties such as freezing range. The mold or slag rim may interact with the shell during the negative strip period, especially if mold friction is large enough to generate significant axial stresses and deformation. Rapid changes in temperature gradient may cause thermal distortion of the shell tip, depending on the mechanical properties of the steel grade. These events are expected to alter the rate of solidification near the meniscus and ultimately dictate the shape and size of sub-surface hooks and OMs.

However, these mechanisms offer conflicting explanations, and are often speculative and incomplete. For example, there is no agreement on when hooks form during the oscillation cycle or if they form by: (i) bending of the initial shell tip [10,11], or (ii) freezing of the liquid steel meniscus [2,5,12–14]. Similarly, differences exist between mechanisms proposed for OMs and surface depressions, which include healing of disjointed steel shell edges [15–17], and mechanical interaction between the mold and shell [18]; and shell bending [10,11] and thermal distortion [19] followed by liquid overflow over the shell tip and subsequent solidification.

Some understanding of initial solidification has come from previous micrographic analyses of hook structure. Emi et al. [10] observed that dendrites initially grow normal to the curved edge of a hook. Within a short distance, they change orientation as heat conduction towards the mold dominates over local heat transfer, and grow roughly perpendicular to the mold walls. Segregation of phosphorus and manganese can be clearly observed along a hook in the microstructures presented by Takeuchi and Brimacombe [2,3] for plain carbon steels ($0.09\% < C < 0.26\%$). They attribute this to a heat-flow effect generated by liquid steel overflowing into the OMs along the casting direction. Harada et al. [8], Yamamura et al. [5], and Yamauchi et al. [20] have compared hook formation in different steel grades. The propensity for hook formation was reported to increase markedly with decreasing carbon content.

A major impediment towards developing a robust understanding of initial solidification is the difficulty of observing hooks in cast samples. Special grade-specific etching reagents are required to reveal clearly the initially solidified structure near the hook, prior to subsequent phase transformations. Previous efforts to observe hook features on slab samples have used either picric acid solution or Oberhoffer's reagent [3]. Although picric acid solution reveals the dendritic structure close to the OM, the hook is difficult to distinguish from the rest of the microstructure. Oberhoffer's reagent relies on the segregation of phosphorus, and can only reveal the linear profile of a hook but not the dendritic structure close to it. Thus, better

etching reagents are needed. Furthermore, the relationship between the dendrite/hook microstructure and the final solidified grain structure has not been investigated in previous work. Scanning electron microscopy (SEM) has not been exploited to study hook formation.

To address the issues mentioned above, the present study was conducted to reveal new information about hook formation in ultralow-carbon steels. Both optical and SEM techniques were used to distinguish simultaneously the hook structure, the surrounding dendrite microstructure, the final grain structure, the grain orientations relative to the hook, and the local composition variations. The results obtained from these different sources reveal unique insights into the sub-surface microstructural evolution during the initial stages of solidification in the meniscus region.

## 2. Experimental

An experimental program was conducted using a conventional continuous slab caster, #2-1 at POSCO Gwangyang Works, South Korea, which features a standard two-port submerged entry nozzle and a 230 mm thick parallel mold with a fully adjustable, non-sinusoidal hydraulic oscillator. Electromagnetic current was employed to control fluid flow conditions in the liquid pool. Table 1 summarizes the casting parameters employed to obtain the various slab samples from the caster. Further details are given elsewhere [21].

The composition of the ultralow-carbon steel grade used during the trials was: Fe with 0.003% C, 0.08% Mn, 0.005% Si, 0.015% P, 0.01% S, 0.01% Cr, 0.01% Ni, 0.01% Cu, 0.05% Ti, and 0.04% Al. The liquidus and solidus temperatures of this steel grade are 1533 and 1517 °C, respectively. The mold powder (Figs. 7 and 8) contained 39.8% CaO, 36.33% $SiO_2$, 6.72% F, 5.97% $Al_2O_3$, 3.43% $Na_2O$, 0.84% MgO, 0.35% $Li_2O$, 0.34% $Fe_2O_3$, 0.18% $TiO_2$, 0.11% $K_2O$, 0.03% $MnO_2$, 1.97% free C, and 3.01% total C. Its melting temperature was 1180 °C and viscosity at 1300 °C was 3.21 Poise.

Samples (100 mm long and encompassing ~10–12 OMs) were obtained near the surface of the narrow faces of 1300 mm wide slabs at five different distances between the wide faces, as shown in Fig. 2. Sections through each sample were cut, mechanically ground, and polished to ~0.25 μm. These were then etched by picric acid solution with additions of the cationic surface-active reagent or surfactant [22] zephiramine (benzyldimethyl-*n*-tetradecylammonium chloride) for ~1–1.5 h. The etching reagent was identified by conducting an intensive experimental program at POSTECH to reveal the solidification microstructure and delineate the hook features in this difficult-to-etch steel grade with ultralow alloy content using optical microscopy. Thus, five micrographs (or two-dimensional (2-D) vertical section views) were obtained from each 3-D hook structure and OM at different locations on the narrow face, as shown in Fig. 2. This figure also shows how the shape of these structures does not vary much with distance along the slab perimeter. Near the corners of the slab, however, the hooks exhibit complex 3-D shapes but metallographic analysis of these effects is beyond the scope of this study.

The distribution of crystallographic orientation in the microstructure near the hook region was analyzed by the electron backscattering diffraction (EBSD) method using a JEOL JSM-7000F® field emission analytical scanning electron microscope. The microscope was equipped with a HKL Technology® EBSD system with a high-resolution (up to 1.2 nm for a 30 kV accelerating voltage) detector that allowed accurate analysis of Kikuchi patterns over an area of 300 μm × 400 μm in steps of 2 μm. The samples were first electropolished using 95% acetic acid–5% perchloric acid solution with a current of 0.2 A for 60 s [23]. The data obtained from EBSD were analyzed using HKL Technology Channel 5® suite of programs, which can display subtle changes in orientation along a line running across grains or sub-grains.

The hook region of samples from a 1960 mm wide slab was also subjected to elemental analysis using the energy dispersive X-ray spectroscopy (EDXS) method using a JEOL JSM-59® scanning electron microscope. To test the possibility of identifying the shape of a hook by obtaining high-resolution elemental maps, electron probe microanalysis (EPMA) of the area of interest was also conducted using a JEOL JXA-8900R® scanning electron microscope.

## 3. Results and discussion

### 3.1. Metallographic assessment of hook shapes

Fig. 3(a) shows a typical "curved" hook adjacent to an OM in one of the slab samples shown in Fig. 1. Each hook has a curved line determined to be the "line of hook origin", which indicates the shape of the meniscus after it solidified. Groups of dendrites growing both away and towards the mold surface from this line can be clearly distinguished, owing to the marked improvement of the current etching method over those methods used in

Table 1
Details of casting parameters for slab samples obtained from POSCO

| Micrograph analysis presented in | Slab width (mm) | Pour temperature (°C) | Casting speed (mm/s) | Mold oscillation frequency (Hz) | Mold oscillation stroke (mm) |
|---|---|---|---|---|---|
| Figs. 3 and 6 | 1300 | 1564 | 28.2 | 3.02 | 6.19 |
| Fig. 4 | 1300 | 1564 | 23.7 | 2.58 | 6.34 |
| Fig. 5 | 1300 | 1565 | 28.2 | 3.02 | 6.18 |
| Figs. 7 and 8 | 1960 | ~1565 | ~16.7 | 1.90 | 5.67 |

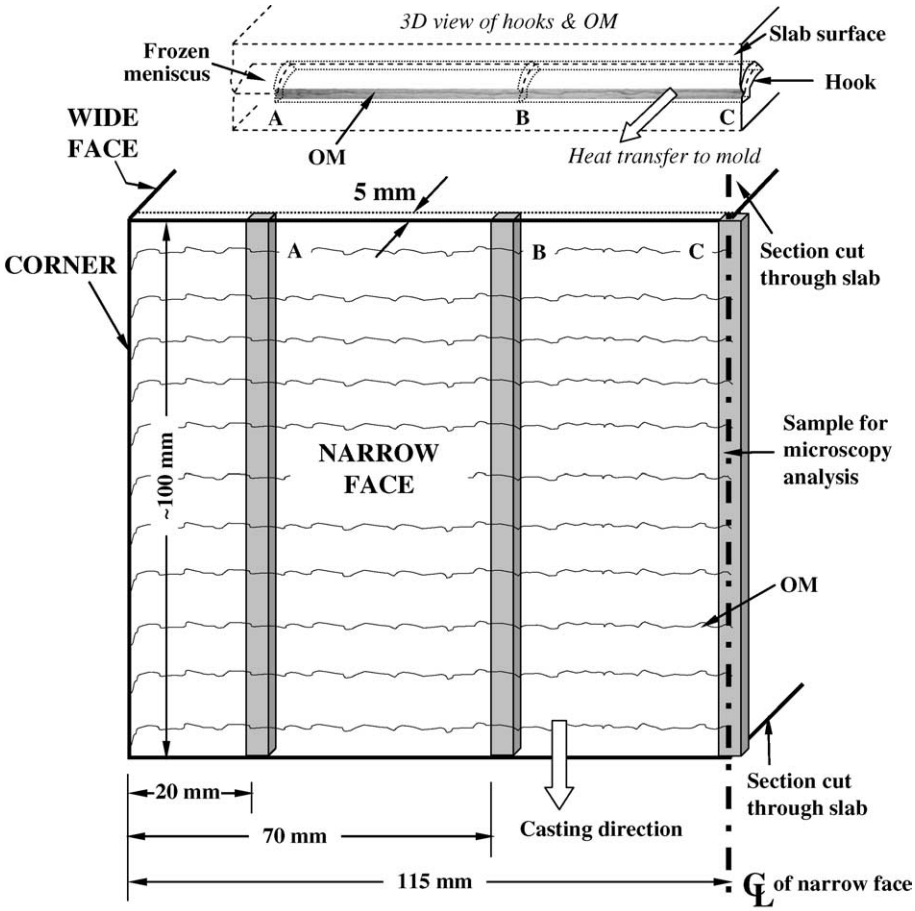


Fig. 2. Schematic showing locations of three samples obtained from a slab section for microscopy analysis of hooks and oscillation marks (OM).

Refs. [3,10]. The characteristic features (e.g., length, depth, and thickness) of the hook can be easily measured from the micrograph. Traces of entrapped argon bubbles and inclusion particles were often found in the vicinity of curved hooks, such as can be seen in this figure. The perpendicular distance from the slab surface to the furthest inner extent of the hook indicates the thickness of surface layer that has to be removed to eliminate the hook and the entrapped bubble.

Fig. 3(b) shows a different curved hook located 35 mm (three OMs away) from the hook in Fig. 3(a). This micrograph illustrates that a portion of the hook can be separated from the solidified meniscus. This indicates brittle fracture (hot tearing) of the fragile semi-solid hook that was likely caused by inertial forces of the molten steel acting during its overflow of the curved hook. This hypothesis is confirmed by the fact that the edges of the outline (estimated initial position) of the separated hook tip and the fractured hook in the figure align almost exactly. Just a small portion of the bottom edge of the hook tip is missing, which appears to have been melted away by the flowing liquid steel. The rest of the hook tip floated away and became entrapped in the solidifying shell growing above the hook. Usually, the fractured shell tip completely melts or is transported away, giving rise to the truncated end observed in most hooks, including the one in Fig. 3(a).

Fig. 4 compares the lines of hook origin (dotted lines) obtained from successive hooks that were observed on a different ~100 mm long steel slab sample. There is a wide variation of hook depth and length, indicating that hook formation is a complex event dictated by the time-dependent meniscus shape as it freezes over the initial shell tip. This observation shows that the shape of the meniscus can be significantly altered during the casting process. This can be attributed to: (i) periodic pressure forces [10,24] generated in the flux channel by the oscillating mold, and (ii) sudden localized metal level fluctuations initiated by chaotic turbulent motion in the molten pool or by abrupt changes in operating conditions.

The lines of hook origin in Fig. 4 are compared with the "no-force" or equilibrium shape of the meniscus, determined solely by the balance of surface tension and ferrostatic pressure forces given by Bikerman's equation [25,26]. In calculating the predicted shape, a surface tension of 1.6 N/m was chosen, corresponding to the sulfur content of 0.01% for the steel grade [27], and the steel density was assumed be 7000 kg/m$^3$ at 1560 °C [28]. A reasonable match between the hook shapes and the shape predicted

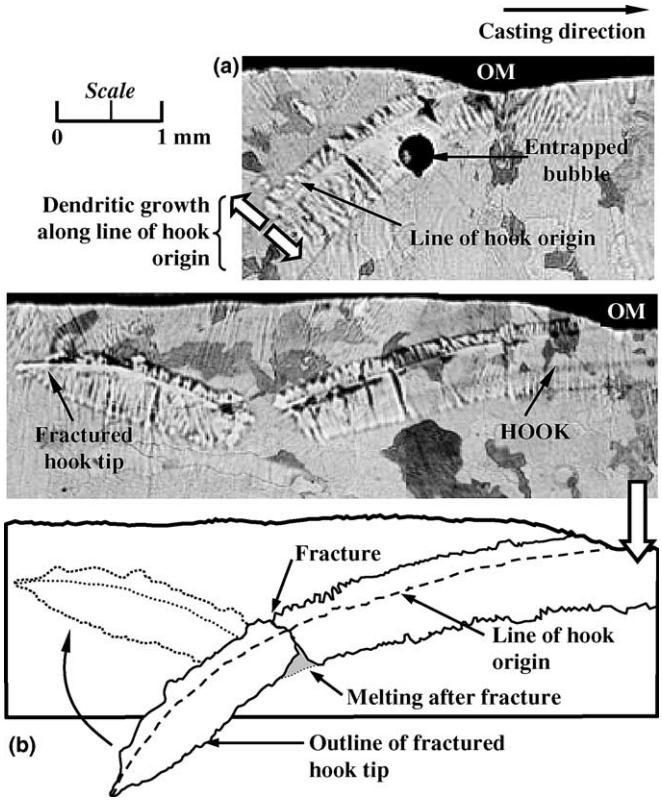


Fig. 3. Hook features in ultralow-carbon steel samples: optical micrographs showing: (a) entrapment of argon bubble by a hook-type oscillation mark (OM), and (b) a fractured hook tip.

by Bikerman's equation confirms that hooks are indeed initiated by meniscus solidification in ultralow-carbon steel slabs. The figure also shows that the hooks are curved much more than the maximum curvature expected from thermal distortion of the initial shell, even for a level fluctuation of 16 mm for 0.4 s [29].

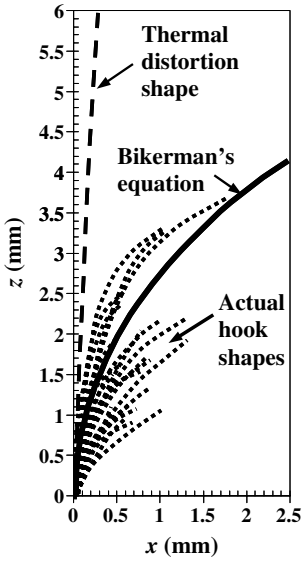


Fig. 4. Comparison between the actual hook shapes, Bikerman's equation, and predicted shell shape after a sudden 16 mm level fluctuation for 0.4 s during the casting process.

The etched hook sample in Fig. 5 clearly reveals dendrites originating from several different nucleation sites located on or near the frozen meniscus (i.e. line of hook origin). Some dendrites grew away from the mold wall. Others grew into the liquid overflow region towards the mold wall, stopped growing, and coarsened. The rest of the overflowed region solidified later, producing a finer structure, as heat was rapidly removed into the mold wall. A group of dendrites growing towards the molten steel abruptly changed direction near the truncated edge, in contrast to the uninterrupted growth in the same direction nearer to the base of the hook. This observation suggests that the truncated hook tip moved when liquid steel overflowed. If meniscus solidification and overflow occur during the negative strip period, it is proposed that the positive pressure in the flux channel can break the hook tip and rotate it slightly [30,31].

### 3.2. Orientation of grains near the hook region

Fig. 6 shows an EBSD map of crystallographic orientations (left) obtained from an area near the line of hook origin for the slab sample shown in Fig. 3(a). The location of this area relative to the hook is also indicated on a back-scattered electron SEM image (right). As an SEM image does not reveal the hook features without etching, the actual hook shape was traced from Fig. 3(a) and transferred to this image.

Grain misorientation plots were obtained along lines (such as (a)–(b) indicated in the figure) running across the grains in the microstructure. By combining the results measured along four different lines, grain misorientations for all of the grains (B–F) relative to the largest grain (A) were calculated and are indicated on the map. It can be clearly seen that the grains below the solid black line have higher relative misorientation than the grains above this line, which is a long grain boundary. The SEM image clearly shows that this line is indeed also a short segment of the line of hook origin. The drastic difference in relative grain orientations can be explained by the fact that solidification above and below the line of hook origin occurred at different times during the oscillation cycle. The lower region solidified first while the interface (meniscus) was covered with mold flux, and then the upper side solidified during subsequent liquid steel overflow.

It is significant that the line of hook origin and the wide difference in relative grain misorientations between the two regions it separates did not disappear even after two subsequent phase transformations (from $\delta$-ferrite to austenite to $\alpha$-ferrite). The persistence of grain boundaries has also been observed by Hunter and Ferry [32] and Takatani et al. [33] during their EBSD characterization studies conducted on stainless steels and Fe–3% Si alloys, respectively. Others [34,35] have seen evidence of grain boundary movement and abnormal grain growth near OMs and surface depressions triggered by shell reheating due to local reduction in heat transfer coefficient. Referring to Fig. 6, it can

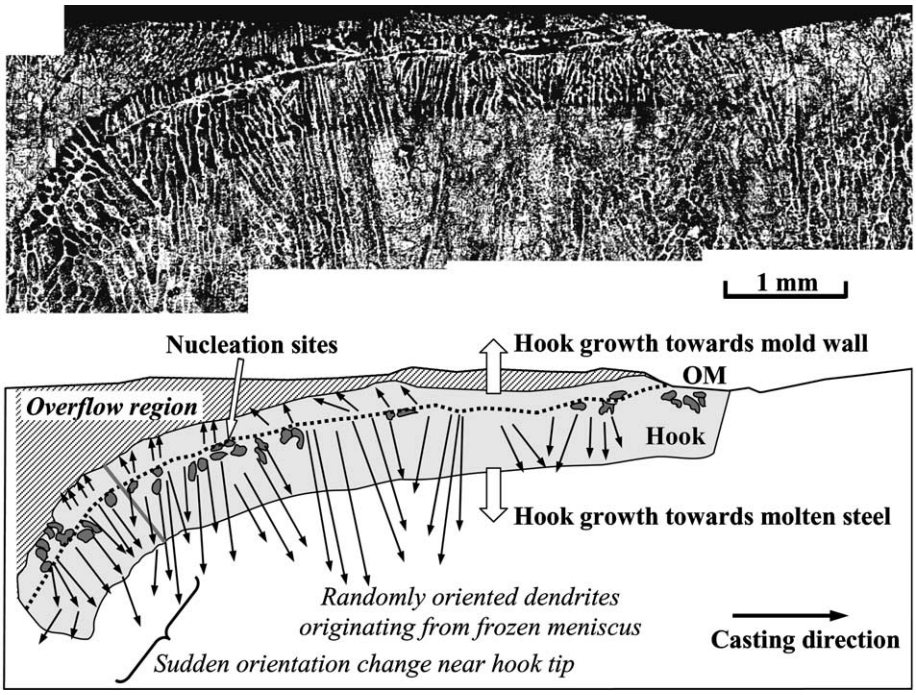


Fig. 5. Optical micrograph of an ultralow-carbon steel sample showing unidirectional growth of dendrites originating from nucleation sites located at the line of hook origin (or frozen meniscus).

be concluded that slightly misoriented grains (such as A and B in the figure) developed due to similar initial dendritic growth. At high temperature, such grains can potentially rotate slightly and thus undergo secondary recrystallization to form very large or ''blown'' grains [36] during the casting process. This will result in a microstructure that is prone to form transverse cracks, which are often observed near the OM roots.

### 3.3. Elemental analysis of the hook region

EDXS analysis was conducted at two regions along the line of hook origin indicated on the SEM image shown in Fig. 7. Traces of fluorine and calcium were detected at areas A and B, respectively. Since these elements are absent in the steel grade being investigated but are present in the mold powder, the appearance of these foreign elements along the line of hook origin can only be explained if the molten flux was retained by the $\delta$-ferrite dendrites growing along the frozen meniscus, prior to liquid steel overflow. Clearly, some mold flux was entrapped by the overflow of liquid steel over the line of hook origin as solidification proceeded rapidly towards the mold wall. The authors believe that the surfactant used in the etching reagent preferentially reacted with the elements present in the mold powder that penetrated between the dendrites, and thus enabled the shape of the hooks and the fractured hook tip in Fig. 3(b) to be revealed by optical microscopy.

The above observation was confirmed by an EPMA map obtained from the same area, which is shown in Fig. 8. The shape of the line of hook origin was clearly revealed (EPMA produces better maps than EDXS area scans) in the elemental map due to the calcium oxide retained along the frozen hook. The corresponding line near the OM valley observed in the SEM image thus is not a ''scratch mark'' produced by improper polishing. High calcium levels near the slab surface indicate that not all of the liquid mold flux that was originally present in this region was displaced by the steel overflow, and ended up being retained in the overflow region.

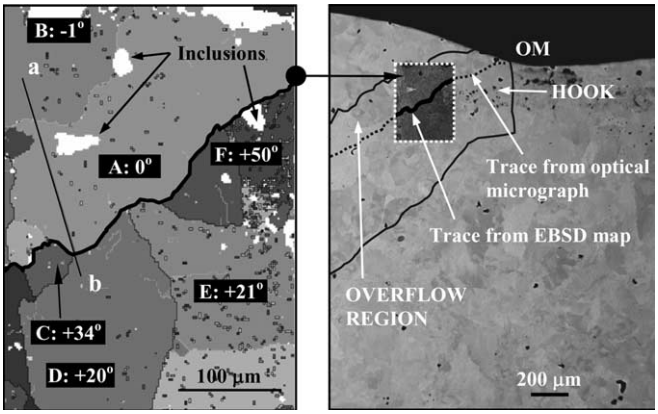


Fig. 6. Electron backscatter diffraction (EBSD) map of grain misorientation measured near the hook shown in Fig. 3(a), and far-away view (backscattered electron image) showing location relative to line of hook origin.

## 4. Implications for hook and OM formation

Simultaneous analysis of the results obtained from both optical microscopy and SEM has revealed new information

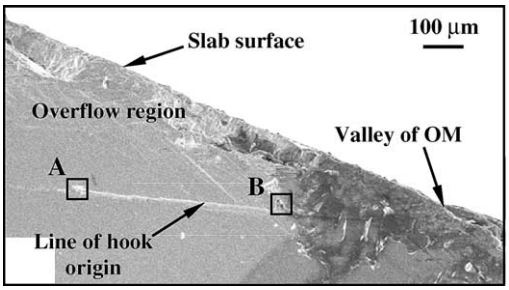


| Element | Area A (wt %) | Area B (wt %) |
|---|---|---|
| C | 5.65 | 16.6 |
| S | 0.22 | --- |
| Mn | 0.68 | --- |
| *F* | *0.81* | --- |
| *O* | --- | *47.16* |
| *Ca* | --- | *33.11* |
| Fe | Bal. | Bal. |

Fig. 7. Energy dispersive X-ray spectroscopy (EDXS) analysis at two locations on the line of hook origin shown on the SEM image reveals traces of fluorine and calcium oxide, which are present in the mold powder but not in the ultralow-carbon steel.

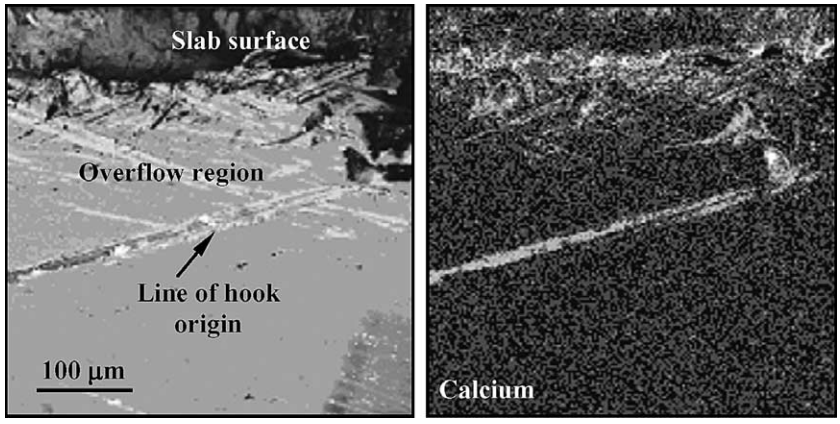


Fig. 8. Electron probe micro analysis (EPMA) near the hook region in the SEM image reveals the line of hook origin on the calcium map.

relating to hook formation in ultralow-carbon steel. This is summarized as follows.

(i) Hook formation is initiated by meniscus solidification. The instantaneous shape of the meniscus at this instant dictates the curvature of the line of hook origin. Recent work has established that this event usually occurs at the beginning of the negative strip period [31]. This is schematically illustrated in Fig. 9(a).

(ii) The hook thickness below the line of hook origin is created by dendritic growth towards the molten steel, originating from nucleation sites along the line of hook origin.

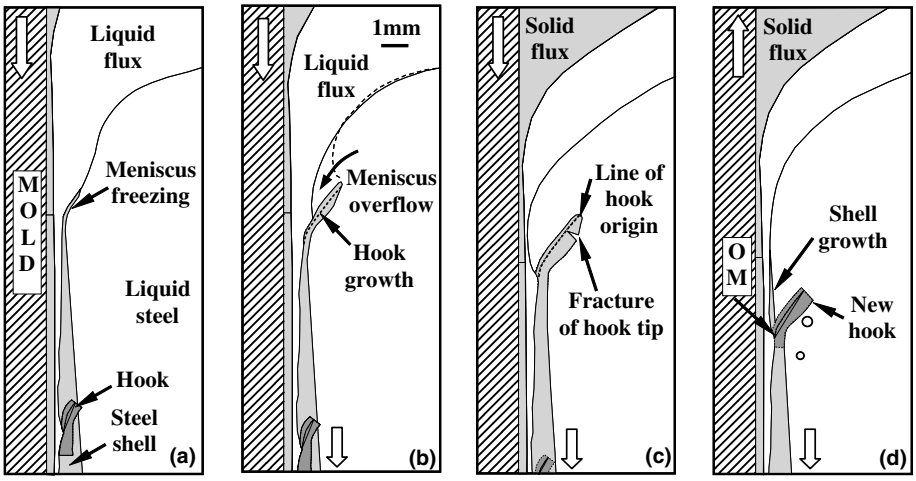


Fig. 9. Schematics illustrating formation of curved hook in an ultralow-carbon steel slab by meniscus solidification and subsequent liquid steel overflow. Oscillation marks (OM) are formed by normal steel shell growth after overflow.

(iii) Some of the molten flux contacts the meniscus (line of hook origin) and penetrates between the dendrites of the solidifying hook, where it is retained and revealed during etching.
(iv) The meniscus subsequently overflows the line of hook origin, as shown in Fig. 9(b). Dendrites quickly grow above the line of hook origin towards the mold wall into the overflowed liquid. The growth stops eventually as the meniscus region gains superheat. The hook edges are established as the dendrites coarsen due to the long local solidification time [31].
(v) Molten flux is retained along the line of hook origin, which is revealed by EDXS analysis and EPMA. Some flux is also retained within the overflowed region.
(vi) The line of hook origin persists as grain boundaries in the final microstructure, despite the occurrence of two separate phase transformations, as revealed by the EBSD analysis. Grains above and below the line of hook origin have distinctly different crystallographic orientations due to the temporal separation between meniscus freezing and liquid overflow.
(vii) The final shape of the hook is completed as the hook tip fractures off and is carried away, as shown in Fig. 9(c).
(viii) The overflow region solidifies forming the OM. The extent of penetration of liquid steel into the flux channel determines the final shape of the upper side of the OM. The hook protruding from the solidifying shell captures inclusions and bubbles in the liquid steel until the shell finally solidifies past the hook. These events are illustrated in Fig. 9(d).

## 5. Conclusion

The sub-surface microstructure of continuous-cast ultra-low-carbon steel slabs has been examined using both optical microscopy and SEM using EBSD, EDXS, and EPMA techniques. Careful selection of an etching reagent allowed the dendrites forming the hook to be clearly distinguished from the rest of the microstructure using optical microscopy. The measured shapes of the line of hook origin matched reasonably well with Bikerman's equation for meniscus shape. This confirms that periodic meniscus solidification during the continuous casting process causes hook formation.

Grain orientation measurements and elemental maps revealed that dendritic growth above the line of hook origin occurs after meniscus overflow over the solidified hook, which also entraps liquid mold flux and persists in the final microstructure. A hook tip that was fractured off, likely during liquid steel overflow, was revealed in the solidified microstructure, and explains the characteristic truncated shape of hooks. Thus, the shape and size of hooks and OMs are determined by two crucial events: (i) the curvature of the line of hook origin as dictated by the instantaneous shape of the meniscus during its solidification, and (ii) the shape of the upper side of the OM, as dictated by the extent of liquid steel overflow. Finally, the microstructural evidence presented here provides the knowledge needed to determine the mechanism of formation of sub-surface hooks and OMs, at least in ultralow-carbon steel slab casting with mold flux.

## Acknowledgements

Financial support from the UIUC Continuous Casting Consortium, National Science Foundation (Grant No. NSF-DMI 04-23794), and POSCO, Gwangyang Works, is acknowledged. The EBSD measurements were carried out in the Center for Microanalysis of Materials, University of Illinois, which is partially supported by the US Department of Energy under Grant DEFG02-91-ER45439. The authors thank Mr. J. Mabon, UIUC Frederick Seitz Materials Research Laboratory, for providing technical support during the EBSD measurements, Prof. H. Henein, University of Alberta, for suggesting the tests, Prof. C.W. Sinclair, Prof. M.A. Wells, and Mr. H. Ahmed, University of British Columbia, for providing initial help with EBSD and sample preparation, and Mr. Go-Gi Lee and Dr. S.M. Kang, POSTECH, for assisting with sample preparation for optical microscopy. Technical support extended by POSCO personnel, i.e. M/s J.M. Park, C.H. Lee, W.Y. Choi, and J.H. Park is also acknowledged.

## References

[1] Brimacombe JK, Sorimachi K. Metall Trans B 1977;8B:489–505.
[2] Takeuchi E, Brimacombe JK. Metall Trans B 1984;15B:493–509.
[3] Takeuchi E, Brimacombe JK. Metall Trans B 1985;16B:605–25.
[4] Suzuki M. CAMP-ISIJ 1998;11:42–4.
[5] Yamamura H, Mizukami Y, Misawa K. ISIJ Int (Suppl) 1996;36:S223–6.
[6] Schmidt KD, Friedel F, Imlau K, Jager W, Muller KT. Steel Res Int 2003;74:659–66.
[7] Birat J-P, Larrecq M, Lamant J-Y, Petegnief J. Steelmaking Conf Proc 1991;74:39–40.
[8] Harada S, Tanaka S, Misumi H, Mizoguchi S, Horiguchi J. ISIJ Int 1990;30:310–6.
[9] Shin H-J, Thomas BG, Lee G-G, Park J-M, Lee C-H, Kim S-H. In: MS&T 2004 Conference Proceedings. New Orleans (LA)/Warrendale (PA): AIST & TMS; 2004. p. 11–26.
[10] Emi T, Nakato H, Iida Y, Emoto K, Tachibana R, Imai T, et al. Proc National Open Hearth Basic Oxygen Steel Conf 1978;61:350–61.
[11] Schwerdtfeger K, Sha H. Metall Mater Trans B 2000;31B:813–26.
[12] Saucedo IG. Steelmaking Conf Proc 1991:43–53.
[13] Bo K, Cheng G, Wu J, Zhao P, Wang J. J Univ Sci Technol Beijing 2000;7:189–92.
[14] Putz O, Breitfeld O, Rodl S. Steel Res 2003;74:686–92.
[15] Szekeres ES. Iron Steel Eng 1996;73:29–37.
[16] Sato R. Proc National Open Hearth and Basic Oxygen Steel Conference 1979;62:48–67.
[17] Savage J, Pritchard WH. Iron Steel 1954;27:649–52.
[18] Brendzy JL, Bakshi IA, Samarasekera IV, Brimacombe JK. Ironmak Steelmak 1993;20:63–74.
[19] Thomas BG, Zhu H. In: Proceedings of JIM/TMS solidification science and processing conference, Honolulu, Hawaii. Warrendale (PA): TMS; 1995. p. 197–208.

[20] Yamauchi A, Itoyama S, Kishimoto Y, Tozawa H, Sorimachi K. ISIJ Int 2002;42:1094–102.
[21] Shin H-J, Lee G-G, Choi W-Y, Kang S-M, Park J-H, Kim S-H. AISTech 2004 iron and steel technology conference proc, vol. II. Nashville (TN)/Warrendale (PA): AIST; 2004. p. 1157–70.
[22] Voort GFV. Mater Charact 1995;35:135–7.
[23] Voort GFV. Metallography: principles and practice. New York (NY): McGraw-Hill; 1984.
[24] Takeuchi S, Miki Y, Itoyama S, Kobayashi K, Sorimachi K, Sakuraya T. Steelmaking Conf Proc 1991:37–41.
[25] Bikerman JJ. Physical surfaces. New York (NY): Academic Press; 1970.
[26] Fredriksson H, Elfsberg J. Scand J Metall 2002;31:292–7.
[27] Lee J, Morita K. ISIJ Int 2002;42:588–94.
[28] Jimbo I, Cramb AW. Iron Steelmaker 1993;20:55–63.
[29] Sengupta J, Thomas BG. In: Continuous Casting Consortium annual report 2005: mathematical models of continuous casting of steel. Urbana (IL): University of Illinois; 2005.
[30] Badri A, Natarajan TT, Snyder CC, Powers KD, Mannion FJ, Cramb A. Metall Mater Trans B 2005;36B:355–71.
[31] Sengupta J, Thomas BG, Shin HJ, Kim SH. Metall Mater Trans A 2005 [submitted].
[32] Hunter A, Ferry M. Scripta Mater 2002;47:349–55.
[33] Takatani H, Gandin CA, Rappaz M. Acta Mater 2000;48:675–88.
[34] Flores O, Martinez L. J Mater Sci 1997;32:5985–91.
[35] Tsai HT, Yin H, Lowry M, Morales S. In: Charlotte NC, editor. AISTech 2005 Proc, vol. II. Warrendale (PA): AISTech; 2005. p. 201–8.
[36] Szekeres ES. In: Sixth international conference on clean steel, Balatonfüred, Hungary; 2002. p. 324–338.